Diagn Interv Radiol 2015; 21:96–104

ABDOMINAL IMAGING
ORIGINAL ARTICLE

Distinguishing intrahepatic cholangiocarcinoma from poorly differentiated hepatocellular carcinoma using precontrast and gadoxetic acid-enhanced MRI

Yoshiki Asayama, Akihiro Nishie, Kousei Ishigami, Yasuhiro Ushijima, Yukihisa Takayama, Nobuhiro Fujita, Yuichiro Kubo, Shinichi Aishima, Ken Shirabe, Takashi Yoshiura, Hiroshi Honda

PURPOSE
We aimed to gain further insight in magnetic resonance imaging characteristics of mass-forming intrahepatic cholangiocarcinoma (mICC), its enhancement pattern with gadoxetic acid contrast agent, and distinction from poorly differentiated hepatocellular carcinoma (pHCC).

METHODS
Fourteen mICC and 22 pHCC nodules were included in this study. Two observers recorded the tumor shape, intratumoral hemorrhage, fat on chemical shift imaging, signal intensity at the center of the tumor on T2-weighted image, fibrous capsule, enhancement pattern on arterial phase of dynamic study, late enhancement three minutes after contrast injection (dynamic late phase), contrast uptake on hepatobiliary phase, apparent diffusion coefficient, vascular invasion, and intrahepatic metastasis.

RESULTS
Late enhancement was more common in mICC (n=10, 71%) than in pHCC (n=3, 14%) ($P < 0.001$). A fat component was observed in 11 pHCC cases (50%) versus none of mICC cases ($P = 0.002$). Fibrous capsule was observed in 13 pHCC cases (59%) versus none of mICC cases ($P < 0.001$). On T2-weighted images a hypointense area was seen at the center of the tumor in 43% of mICC (6/14) and 9% of pHCC (2/22) cases ($P = 0.018$). Other parameters were not significantly different between the two types of nodules.

CONCLUSION
The absence of fat and fibrous capsule, and presence of enhancement at three minutes appear to be most characteristic for mICC and may help its differentiation from pHCC.

From the Departments of Radiology (Y.A. ✉ *asayama@radiol.med.kyushu-u.ac.jp*, A.N., K.I., Y.U., N.F., T.Y., H.H.), Molecular Imaging & Diagnosis (Y.T.), Anatomic Pathology (N.F., Y.K., S.A.), Surgery and Science (K.S.), Kyushu University Graduate School of Medical Sciences, Fukuoka, Japan.

Received 23 April 2014, revision requested 29 June 2014, final revision received 3 September 2014, accepted 24 September 2014.

Published online 16 February 2015.
DOI 10.5152/dir.2014.13013

Intrahepatic cholangiocarcinomas (ICC) are primary liver cancers composed of carcinoma cells that resemble biliary epithelial cells surrounded by fibrous stroma of various degrees. The Japanese Liver Cancer Group has classified ICCs into three types: mass-forming, periductal-infiltrative, and intraductal (1). The mass-forming type of intrahepatic cholangiocarcinoma (mICC) is the most common (60% of all ICCs) (2) and can show various imaging findings on dynamic computed tomography (CT) or magnetic resonance imaging (MRI) using extracellular contrast agent (3, 4). Regardless of the findings on the arterial phase, delayed temporal contrast enhancement is a typical feature of ICC because of the distribution of extracellular contrast into intratumoral fibrous stroma (5).

Intratumoral fat is an important diagnostic clue for hepatocellular carcinoma (HCC) and is frequently seen in well-differentiated HCCs (6). However, the frequency of this finding has not been well evaluated in poorly differentiated HCCs (pHCC). From the standpoint of tumor vascularity, the arterial blood supply significantly decreases as the histological grade increases in the late stage of HCC development (7). Thus, pHCC can show hypovascularity or ring-like enhancement, which sometimes mimics that of mICC. Despite the similarity of imaging findings on the arterial phase, delayed washout of pHCC can enable its differentiation from mICC when the examination is performed using an extracellular contrast agent. In spite of their similarities in preoperative imaging, hepatic resection is the only curative option for mICC, while other treatments such as radiofrequency ablation and transcatheter arterial chemoembolization can be alternative treatment options for pHCC. Thus, it is important to differentiate mICC from pHCC. Colorectal cancer metastasis is another main differential diagnosis, but usually it is easily diagnosed from the patients' history.

Several reports have demonstrated that there is a significant difference in ADC between benign and malignant lesions and that the mean ADC of benign lesions is higher than that of malignant lesions (8). Radiologically, mICC is expected to be hypointense on T1-weighted images, hyperintense with central hypointensity on T2-weighted images, with no signal drop-off on chemical shift imaging and a low ADC value. Typically, pHCC is also hypointense on T1-weighted images, hyperintense on T2-weighted images, with or without signal drop-off on chemical shift imaging and a low ADC value. Thus, it seems to be difficult to differentiate mICC from pHCC on conventional MRI.

Gadoxetic acid, a recently developed hepatobiliary contrast agent, has become available for detection and characterization of focal hepatic lesions, and its usefulness has been reported by many researchers (9).

As approximately 50% of the administered dose of this agent is taken up by functional hepatocytes, focal liver lesions without functional hepatocytes are hypointense (no uptake) on hepatobiliary phase (about 20 minutes after injection), in which contrast washout phenomenon is not valid with hepatobiliary agents. Thus, even though some HCC can show the uptake of gadoxetic acid (10), both mICC and pHCC are expected to show hypointense lesions in the hepatobiliary phase, making them indistinguishable from each other. Furthermore, the presence of a fibrous capsule, a characteristic finding of classic HCC (11), cannot be evaluated on hepatobiliary phase. On the other hand, gadoxetic acid also works as an extracellular contrast agent for the first few minutes (12, 13). To the best of our knowledge, there are no reports of the late phase (three to five minutes after contrast injection) imaging features of liver tumors on gadoxetic acid-enhanced MRI.

The aim of this study was to retrospectively determine unenhanced and gadoxetic-acid enhanced late phase imaging findings of mICC, with a special focus on distinguishing these findings from those of pHCC.

Methods

Patients

We identified 239 consecutive patients with surgically resected or explanted ICC or HCC at our hospital from June 2008 to May 2011. Sclerosing HCC or mucinous-type ICC patients were not found in this period. Eighteen cases of combined HCC and ICC were excluded. Based on the definitions provided by the Japanese Liver Cancer Group (1), 14 cases were mICC and 25 cases were pHCC. Patients who had undergone MRI without gadoxetic acid were excluded (three pHCC lesions). Thus, a total of 36 patients (14 patients with mICC lesions and 22 patients with pHCC lesions) were retrospectively selected for this study. Clinical data were obtained on serum viral markers (hepatitis B and hepatitis C), chronic liver disease, and Child-Pugh class. Patients with positive serologic results for hepatitis B surface antigen, antibody to hepatitis B core antigen, or anti-hepatitis C virus were considered to be positive for serum viral markers. Chronic liver disease was considered present when the viral marker result was positive or chronic hepatitis or cirrhosis was documented in the medical records or pathological reports.

Pathological evaluation

Two experienced pathologists (N.F. and S.I., with four and 13 years of experience, respectively) examined the resected specimens of all 36 cases. All specimens were fixed with formalin and cut to a thickness of 5 mm in the transverse plane, similar to axial MRI sections. Signs of fibrous capsule and intratumoral fibrous desmoplasia were evaluated and compared with MRI findings.

MRI protocol

MRI sequences are summarized in Table 1. MRI was performed for all patients using a superconducting magnet operating at 1.5 T (Intera Achieva Nova Dual; Philips Healthcare) or 3.0 T (Achieva, Quasar Dual, Philips Healthcare) with a sensitivity-encoding (SENSE) body coil, including axial in-phase and out-of-phase T1-weighted gradient-echo images (chemical shift imaging, CSI), single-shot T2-weighted spin-echo images with or without fat suppression, and diffusion-weighted single-shot spin-echo echo-planar images. Apparent diffusion coefficient (ADC) maps were automatically generated on the operating console using all three images with b-factors of 0, 500, and 1000 s/mm^2. Dynamic fat-suppressed T1-weighted gradient-echo images with a three-dimensional acquisition sequence (T1-high resolution isotropic volume excitation [THRIVE]) were obtained using fluoroscopic triggering (Bolus Trak, Philips Medical Systems) before (precontrast) and at 18–25 s (arterial phase), 55–60 s (portal-venous phase), 90 s (venous phase), 3 min (dynamic late phase (14), 10 min, and 20 min following the administration of gadoxetic acid (Gadolinium-ethoxylbenzyl-diethylenetriamine pentaacetic acid, Primovist, Bayer). Gadoxetic acid was administered as a bolus dose at a rate of 2 mL/s (0.025 mmol/kg body weight) through an IV cubital line (22-gauge)

Table 1. MRI sequences and parameters for 1.5 T and 3.0 T imaging systems

1.5 T	Unit	CSI	ssT2WI	DWI	THRIVE
Repetition time	ms	185.0	4345.0	1542.0	3.6
Echo time	ms	2.3/4.6	90.0	71	1.8
Flip angle	degree	75	90	90	18
Slice thickness	mm	7.0	7.0	7.0	3.0
Slice gap	mm	1.0	1.0	1.0	1.5
Number of excitations		1	2	1	1
Field of view	mm	360×298	360×283	360×304	360×252
Matrix size		256×148	224×123	128×70	240×168
3.0 T	**Unit**	**CSI**	**ssT2WI**	**DWI**	**eTHRIVE**
Repetition time	ms	148.0	1445.0	1867.0	3.0
Echo time	ms	1.2/2.0	70.0	55.0	1.4
Flip angle	degree	60	90	90	10
Slice thickness	mm	7.0	7.0	7.0	3.0
Slice gap	mm	1.0	1.0	1.0	1.5
Number of excitations		1	1	1	1
Field of view	mm	380×329	380×299	380× 299	375×298
Matrix size		240×207	112×88	112×88	252×200

CSI, chemical shift imaging; ssT2WI, single-shot T2-weighted spin-echo images; DWI, diffusion weighted images; THRIVE, T1-high resolution isotropic volume excitation; eTHRIVE, enhanced T1-high resolution isotropic volume excitation.

that was flushed with 20 mL saline using a power injector.

Image evaluation

Images of all axial sections of the tumor were evaluated in consensus by two radiologists (A.N. and K.I. with 17 and 16 years of experience in abdominal MRI, respectively). The reviewers were blinded to the pathological and clinical data. Qualitative image analysis included assessment of shape, intratumoral hemorrhage, fat, central hypointensity on T2-weighted images, fibrous capsule, arterial enhancement pattern, late enhancement, uptake of contrast on hepatobiliary phase (20 minutes after contrast injection), vascular invasion, and intrahepatic metastasis. The ADC value was also measured.

Lesion shape was classified as lobulated or round-oval. Intratumoral hemorrhage was identified by high signal intensity on CSI without signal drop-off together with absence of contrast enhancement. The presence of fat was identified by a signal drop-off on CSI. A fibrous capsule was identified by a hypointense rim having a thickness of 2 mm or more and encircling the lesion at the periphery on either a precontrast gradient-echo image or T2-weighted images. Rim enhancement seen on the dynamic late phase was also judged as a fibrous capsule. The arterial enhancement pattern was classified as ring-like or other. Late enhancement was defined as an area of gradually increasing intensity on the dynamic late phase image compared with that on precontrast and arterial phases. Positive uptake of contrast on hepatobiliary phase was qualitatively defined as higher intensity than those in the precontrast scan. The ADC value of each tumor was measured by placing a region of interest (ROI) on the ADC map. The largest possible round or oval ROI with an area of at least 0.7 cm^2 was placed on the solid region where the ADC was considered to be the lowest in the entire tumor. Regions of hemorrhage, degeneration, or necrosis were avoided by referring to the CSI, T2-weighted images, and contrast sequences. Nodules that were invisible on the ADC map were localized on other MRI sequences and correlated with the ADC map. When it was difficult to determine the lowest ADC region visually, the minimum value was recorded after placing ROIs on several regions that the three radiologists judged to show a low ADC. Other findings such as capsular retraction, signs of cirrhosis, and lymphadenopathy were not included because these findings were additional and not inherent.

Statistical analysis

Continuous variables were expressed as mean±standard deviation (SD) and were tested using the Student's t test. Tumor markers were expressed as median (minimum and maximum) and were tested using the Mann-Whitney U test. Categorical variables were tested using the Fisher's exact test. A difference with a *P* value less than 0.05 was considered statistically significant for all tests. JMP Pro version 11 (SAS Institute) was used for analyses.

Results

Patient characteristics are shown in Table 2. We observed a significant difference in chronic liver disease distribution between the mICC and pHCC groups (P = 0.006). However, six of 14 cases (42.9%) also had background liver disease, even in the mICC group. The two groups had no significant difference in age, gender, or Child-Pugh class distribution. There were no cases of Child-Pugh class C. None of the patients had large amounts of ascites.

Twenty-six cases (11 mICC and 15 pHCC) were examined by 1.5 T scanner and 10 cases (three mICC and seven pHCC) were examined by 3.0 T scanner. Previous investigators reported that 3.0 T MRI is similar to 1.5 T MRI for various outcomes (15), thus no significant difference was to be expected between 1.5 T and 3.0 T. MRI results are shown in Table 3. Lobulated shape was seen in eight mICC cases (57%) and five pHCC cases (23%), respectively (P = 0.036). A fat component was observed in 11 pHCC cases (50%) versus none of mICC cases (P = 0.002). Fibrous capsule was observed in 13 pHCC cases (59%) versus none of mICC cases

Table 2. Patient characteristics

	mICC (n=14)	pHCC (n=22)	*P*
Age (years), mean±SD	62.4±9.8	58.5±13.5	0.362
Gender (M:F)	10:4	18:4	0.465
Chronic liver disease, n (%)	6 (42.9%)	20 (90.9%)	0.006
Etiology, n			
Hepatitis B/C	4	17	
Alcoholic	0	1	
NASH	0	1	
Banti syndrome	1	0	
Unknown	1	1	
Child-Pugh, n			
A	13	21	1.000
B	1	1	
Tumor markers, median (min–max)			
AFP (ng/mL)	3.7 (2.1–30.1)	393.2 (2.3–994600)	<0.001
DCP (mAU/mL)	26 (9–571)	1329.5 (13–109730)	0.013
CEA (ng/mL)	3.5 (0.4–63.6)	2.5 (0.8–5.7)	0.077
CA 19-9 (U/mL)	44.1 (7.4–287228)	26.9 (1.4–49.7)	0.156

mICC, mass-forming intrahepatic cholangiocarcinoma; pHCC, poorly differentiated hepatocellular carcinoma; M, male; F, female; NASH, nonalcoholic steatohepatitis; AFP, alpha-fetoprotein; DCP, des-gamma-carboxy prothrombin; CEA, carcinoembryonic antigen; CA19-9, carbohydrate antigen 19-9.

Cutoff values: AFP 6.2 ng/mL; DCP, 40 mAU/mL; CEA, 3.2 ng/mL; CA19-9, 37 U/Ml.

Table 3. Patient characteristics

	mICC (n=14)	pHCC (n=22)	*P*
Size (cm), mean±SD (min–max)	5.0±2.4 (1.5–7.5)	7.5±4.7 (2.0–16.5)	0.066
Shape			
Lobulated	8 (57)	5 (23)	0.036
Round/oval	6 (43)	17 (77)	
Intratumoral hemorrhage	4 (29)	11(50)	0.204
Fat	0 (0)	11 (50)	0.002
Central hypointensity on T2WI	6 (43)	2 (9)	0.018
Fibrous capsule	0 (0)	13 (59)	<0.001
Arterial enhancement			
Ring-like	11 (79)	11 (50)	0.087
Other	3 (21)	11 (50)	
Late enhancement	10 (71)	3 (16)	<0.001
Uptake on hepatobiliary base	4 (19)	2 (9)	0.126
ADC value ($\times 10^{-3}$ mm^2/s), mean±SD	0.85±0.18	0.87±0.20	0.722
Vascular invasion	2 (14)	4 (18)	0.760
Intrahepatic metastasis	3 (21)	8 (36)	0.343

Data are presented as n (%), unless otherwise noted.

mICC, mass-forming intrahepatic cholangiocarcinoma; pHCC, poorly differentiated hepatocellular carcinoma; SD, standard deviation; T2WI, T2-weighted imaging; ADC, apparent diffusion coefficient.

($P < 0.001$, Fig. 1); hypointense rim on precontrast T1-weighted image and T2-weighted image were detected in 10 and five cases, respectively. Rim enhancement on the dynamic late phase was seen in three cases. A hypointense area on T2-weighted image was seen at the center of the tumor in six of 14 mICC cases (43%) and two of 22 pHCC cases (9%), respectively ($P = 0.018$). Late enhancement was more commonly observed in mICC (n=10, 71%) than in pHCC (n=3, 14%) ($P < 0.001$) (Figs. 2, 3). No significant difference was observed in terms of intratumoral hemorrhage, arterial enhancement pattern (Figs. 2, 3), uptake of contrast on the hepatobiliary phase, ADC value, vascular invasion, or intrahepatic metastasis.

In pathological evaluation, central fibrous desmoplasia was observed to a greater or lesser degree in all mICC cases, while it was not observed in any pHCC cases. Pathologically, a fibrous capsule was detected in none of 14 mICC cases and 21 of 22 pHCC cases (95%). Of these 21 pHCC cases with pathologically identified fibrous capsule, MRI could identify the fibrous capsule during precontrast T1-weighted phase in 10 patients (47.6%), T2-weighted phase in five patients (23.8%), and dynamic late phase in three patients (14.3%).

Discussion

In this study MRI revealed interesting differences between mICC and pHCC, particularly relating to the presence or absence of intratumoral fat and fibrous capsule, and late enhancement at three minutes after hepatobiliary contrast agent injection.

It is well known that HCC has various degrees of fatty metamorphosis. However, researchers have focused on its relationship in the course of early stage of hepatocarcinogenesis. Fatty change is an important marker for the transformation of premalignant lesions to hepatocellular carcinoma (16). There are few reports regarding the fatty change of pHCC. Pathological evaluation by Kutami et al. (6) revealed frequencies of fatty change in well differentiated HCC, well-to-moderately differentiated HCC, moderately differentiated HCC, and moderately-to-poorly differentiated HCC as 42.0%, 37.5%, 6.0%, and 0%, respectively. Our study showed that there is a relatively high frequency of fatty change in pHCC (50%). The mechanism of fatty change in pHCC has not been reported previously. In case of small HCC (mainly well differentiated HCC), fatty change is closely related to an insufficient development of the arterial tumor vessels (6). Arterial blood supply significantly decreases as the histological grade increases in the late stage of HCC development (from moderately differentiated HCC to pHCC) (7), which may be related to the high frequency of fatty change in pHCC.

The imaging features of ICC have been reported by many researchers (3, 4). Most of these focused on imaging characteristics in relation to the internal desmoplastic change. Maetani et al. (4) observed central hypointensity on T2-weighted images in 27 of 50 cases (54%) of ICC and suggested that this finding, which reflects severe fibrosis, may be a characteristic marker of ICC. In our study, a central hypointense area was seen on T2-weighted images in six of 14 cases (42.9 %), which is concordant with their results. The number of cases exhibiting hypointensity on T2-weighted images (n=6) was lower than that of late enhancement (n=10) in the present study. Coagulation necrosis shows both high and low signal intensity on T2-weighted images and can intermingle with the fibrous stroma, which can affect the internal signal intensity. Another potential cause of this discrepancy may have been the scanning slice thickness (7 mm vs. 3 mm) and contrast resolution.

The standard gadolinium dose for gadoxetic acid (0.025 mmol/kg) is one-fourth that of gadopentetate dimeglumine (0.1 mmol/kg). As the T1 relaxivity of gadoxetic acid is 1.8 times that of gadopentetate dimeglumine (17), the expected T1 relaxation effect would be expected to be one-half that of gadopentetate dimeglumine (18). Biodistribution studies of gadoxetic acid have shown dose-independent renal (41.6%–51.2%) and biliary (43.1%–53.2%) elimination and an enterohepatic recirculation rate of approximately 4% (19). Even though

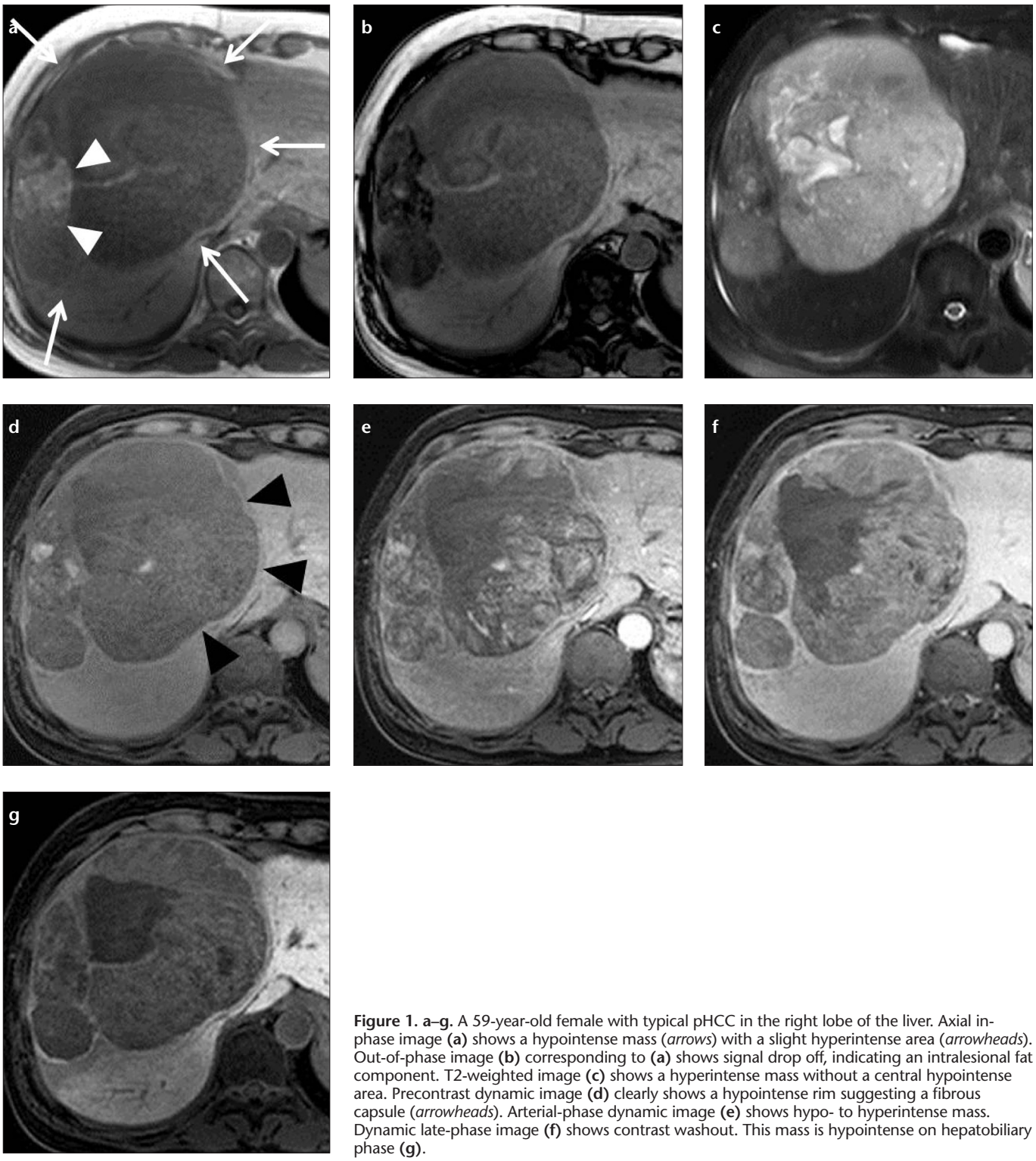

Figure 1. a–g. A 59-year-old female with typical pHCC in the right lobe of the liver. Axial in-phase image **(a)** shows a hypointense mass (*arrows*) with a slight hyperintense area (*arrowheads*). Out-of-phase image **(b)** corresponding to **(a)** shows signal drop off, indicating an intralesional fat component. T2-weighted image **(c)** shows a hyperintense mass without a central hypointense area. Precontrast dynamic image **(d)** clearly shows a hypointense rim suggesting a fibrous capsule (*arrowheads*). Arterial-phase dynamic image **(e)** shows hypo- to hyperintense mass. Dynamic late-phase image **(f)** shows contrast washout. This mass is hypointense on hepatobiliary phase **(g)**.

the effect of recirculated or extracellular distribution of gadolinium might be less in gadoxetic acid-enhanced MRI than in gadopentetate dimeglumine-enhanced MRI, our result suggests that the dynamic late phase can give us useful information, similar to delayed enhancement, using an extracellular contrast agent. In addition, despite the absence of functional hepatocytes in mICC, uptake of contrast was seen in four mICC cases on hepatobiliary phase. This is probably due to the remaining contrast in the extracellular space of the tumor. After 2–5 minutes of contrast injection, extracellular contrast agent returns from the interstitial space to the vascular space due to decreased concentration in the vascular space caused by excretion into urine (20). Furthermore, because of the

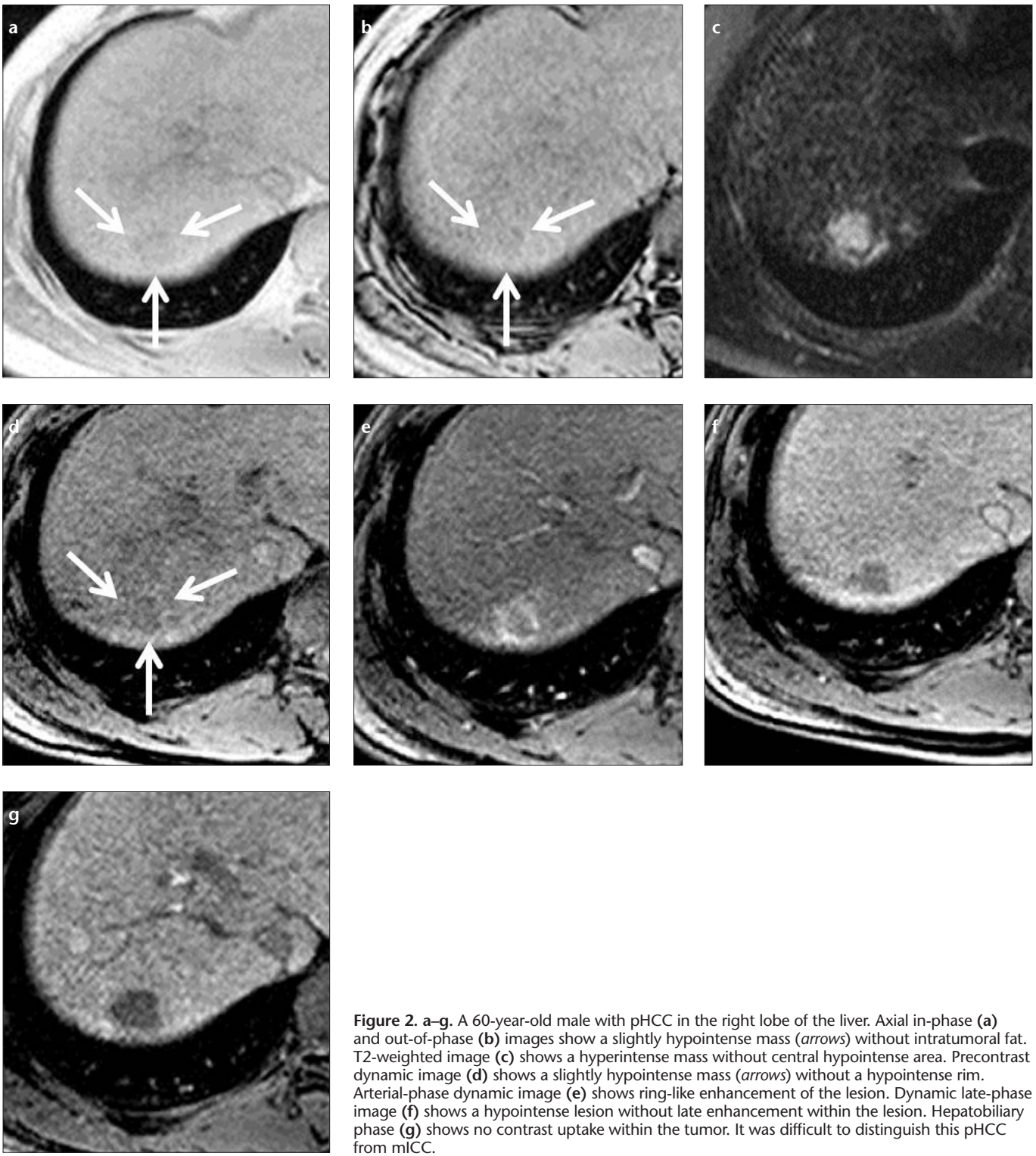

Figure 2. a–g. A 60-year-old male with pHCC in the right lobe of the liver. Axial in-phase **(a)** and out-of-phase **(b)** images show a slightly hypointense mass (*arrows*) without intratumoral fat. T2-weighted image **(c)** shows a hyperintense mass without central hypointense area. Precontrast dynamic image **(d)** shows a slightly hypointense mass (*arrows*) without a hypointense rim. Arterial-phase dynamic image **(e)** shows ring-like enhancement of the lesion. Dynamic late-phase image **(f)** shows a hypointense lesion without late enhancement within the lesion. Hepatobiliary phase **(g)** shows no contrast uptake within the tumor. It was difficult to distinguish this pHCC from mICC.

stronger enhancement of the liver parenchyma on hepatobiliary phase of gadoxetic acid-enhanced image (21), most mICC did not show contrast distribution, in contrast to dynamic late phase. In case of pHCC, the uptake of contrast was observed only in 9% of cases (2 of 22) on hepatobiliary phase, because the expression of uptake transporter (organic anion-transporting polypeptide 8 (OATP8) may decrease as the tumor grade advances (22). Hepatobiliary phase images were not helpful in differentiating mICC from pHCC in our study, however, hepatobiliary phase is very useful in detection of satellite nodules or intrahepatic metastases (21). In addition, radiologists should pay attention to the pseudo-washout sign (23), which shows relatively low signal intensi-

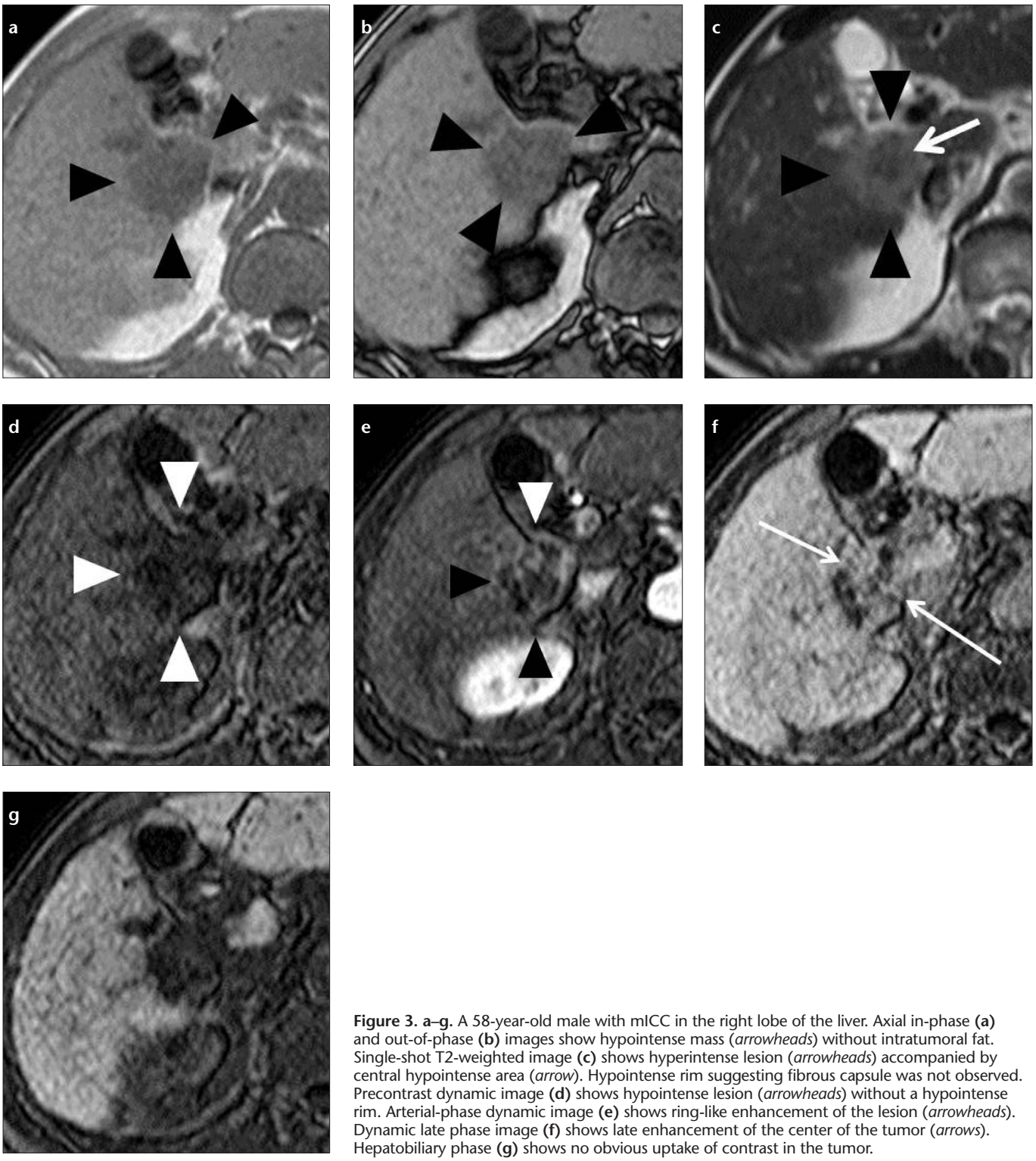

Figure 3. a–g. A 58-year-old male with mICC in the right lobe of the liver. Axial in-phase **(a)** and out-of-phase **(b)** images show hypointense mass (*arrowheads*) without intratumoral fat. Single-shot T2-weighted image **(c)** shows hyperintense lesion (*arrowheads*) accompanied by central hypointense area (*arrow*). Hypointense rim suggesting fibrous capsule was not observed. Precontrast dynamic image **(d)** shows hypointense lesion (*arrowheads*) without a hypointense rim. Arterial-phase dynamic image **(e)** shows ring-like enhancement of the lesion (*arrowheads*). Dynamic late phase image **(f)** shows late enhancement of the center of the tumor (*arrows*). Hepatobiliary phase **(g)** shows no obvious uptake of contrast in the tumor.

ty of hypervascular tumor because of continuous contrast uptake in the surrounding normal hepatic parenchyma during the equilibrium phase.

MRI detection of fibrous capsule using an extracellular contrast agent is reported to be most sensitive on the delayed-phase (24). Our results showed that precontrast T1-weighted image is the most sensitive at detecting fibrous capsule, while dynamic late phase had the lowest detection rate. Even though there is a fair amount of contrast distribution into the fibrous capsule, increasing signal intensity due to uptake of contrast by the hepatocytes and excretion into bile ducts in the surrounding noncancerous parenchyma may obscure the pseudocapsule (Fig. 4).

Nishie et al. (25) reported that the mean ADC of pHCC is significantly low-

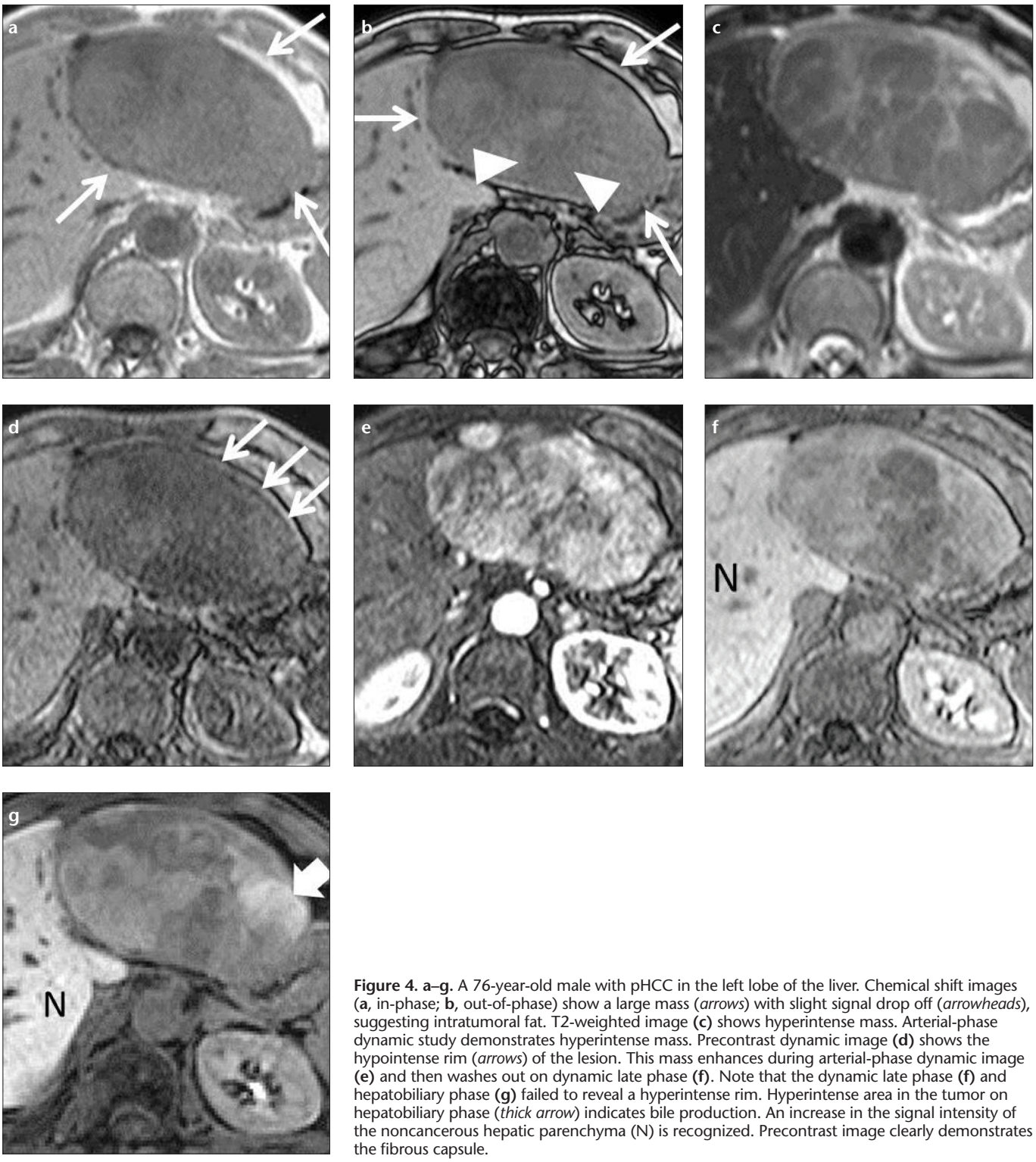

Figure 4. a–g. A 76-year-old male with pHCC in the left lobe of the liver. Chemical shift images (**a**, in-phase; **b**, out-of-phase) show a large mass (*arrows*) with slight signal drop off (*arrowheads*), suggesting intratumoral fat. T2-weighted image **(c)** shows hyperintense mass. Arterial-phase dynamic study demonstrates hyperintense mass. Precontrast dynamic image **(d)** shows the hypointense rim (*arrows*) of the lesion. This mass enhances during arterial-phase dynamic image **(e)** and then washes out on dynamic late phase **(f)**. Note that the dynamic late phase **(f)** and hepatobiliary phase **(g)** failed to reveal a hyperintense rim. Hyperintense area in the tumor on hepatobiliary phase (*thick arrow*) indicates bile production. An increase in the signal intensity of the noncancerous hepatic parenchyma (N) is recognized. Precontrast image clearly demonstrates the fibrous capsule.

er than those of well and moderately differentiated HCC. To our knowledge, no previous reports focusing on the ADC of mICC have been reported. In our study, the mean ADC of mICC (0.85±0.18 $\times 10^{-3}$ mm^2/s) was almost the same as that of pHCC (0.87±0.20 $\times 10^{-3}$ mm^2/s). We can deduce from these data that it is difficult to differentiate mICC from pHCC by means of ADC.

There were several limitations to this study. First, our study population was small because mICC and pHCC are not common diseases. Second, we did not compare the area of late enhancement to that of pathological fibrosis directly. Third, in daily practice, dynamic CT is routinely performed for evaluating liver tumor; thus, delayed enhancement can be easily evaluated. We did not directly compare the

diagnostic performance of gadoxetic acid-enhanced MRI and dynamic CT or extracellular gadolinium contrast agent. Fourth, we did not compare with other tumors such as liver metastasis or inflammatory pseudotumor in noncirrhotic liver. In particular, liver metastasis in noncirrhotic liver will be encountered in the daily practice. It goes without saying that patients' medical history is important in making the differential diagnosis.

In conclusion, the absence of fat and fibrous capsule, and presence of enhancement at 3 min are more indicative for mICC than for pHCC.

Acknowledgements

This work was supported by JSPS KAKENHI Grant Number 22591343.

Conflict of interest disclosure

The authors declared no conflicts of interest.

References

1. The Liver Cancer Study Group of Japan. The general rules for the clinical and pathological study of primary liver cancer. 5th ed. Tokyo: Kanehara, 2008.
2. Lim JH. Cholangiocarcinoma: morphologic classification according to growth pattern and imaging findings. AJR Am J Roentgenol 2003; 181:819–827. [CrossRef]
3. Asayama Y, Yoshimitsu K, Irie H, et al. Delayed-phase dynamic CT enhancement as a prognostic factor for mass-forming intrahepatic cholangiocarcinoma. Radiology 2006; 238:150–155. [CrossRef]
4. Maetani Y, Itoh K, Watanabe C, et al. MR imaging of intrahepatic cholangiocarcinoma with pathologic correlation. AJR Am J Roentgenol 2001; 176:1499–1507. [CrossRef]
5. Lacomis JM, Baron RL, Oliver JH 3rd, Nalesnik MA, Federle MP. Cholangiocarcinoma: delayed CT contrast enhancement patterns. Radiology 1997; 203:98–104. [CrossRef]
6. Kutami R, Nakashima Y, Nakashima O, Shiota K, Kojiro M. Pathomorphologic study on the mechanism of fatty change in small hepatocellular carcinoma of humans. J Hepatol 2000; 33:282–289. [CrossRef]
7. Asayama Y, Yoshimitsu K, Nishihara Y, et al. Arterial blood supply of hepatocellular carcinoma and histologic grading: radiologic-pathologic correlation. AJR Am J Roentgenol 2008; 190:W28–34. [CrossRef]
8. Bruegel M, Holzapfel K, Gaa J, et al. Characterization of focal liver lesions by ADC measurements using a respiratory triggered diffusion-weighted single-shot echo-planar MR imaging technique. Eur Radiol 2008; 18:477–485. [CrossRef]
9. Ringe KI, Husarik DB, Sirlin CB, Merkle EM. Gadoxetate disodium-enhanced MRI of the liver: part 1, protocol optimization and lesion appearance in the noncirrhotic liver. AJR Am J Roentgenol 2010; 195:13–28. [CrossRef]
10. Asayama Y, Tajima T, Nishie A, et al. Uptake of Gd-EOB-DTPA by hepatocellular carcinoma: radiologic-pathologic correlation with special reference to bile production. Eur J Radiol 2011; 80:e243–248. [CrossRef]
11. Ishigami K, Yoshimitsu K, Nishihara Y, et al. Hepatocellular carcinoma with a pseudocapsule on gadolinium-enhanced MR images: correlation with histopathologic findings. Radiology 2009; 250:435–443. [CrossRef]
12. Clement O, Muhler A, Vexler V, Berthezene Y, Brasch RC. Gadolinium-ethoxybenzyl-DTPA, a new liver-specific magnetic resonance contrast agent. Kinetic and enhancement patterns in normal and cholestatic rats. Invest Radiol 1992; 27:612–619. [CrossRef]
13. Tsuda N, Kato N, Murayama C, Narazaki M, Yokawa T. Potential for differential diagnosis with gadolinium-ethoxybenzyl-diethylenetriamine pentaacetic acid-enhanced magnetic resonance imaging in experimental hepatic tumors. Invest Radiol 2004; 39:80–88. [CrossRef]
14. Tanimoto A, Lee JM, Murakami T, Huppertz A, Kudo M, Grazioli L. Consensus report of the 2nd International Forum for Liver MRI. Eur Radiol 2009; 19 (Suppl 5):S975–989. [CrossRef]
15. Wood R, Bassett K, Foerster T, Spry C, Tong L. 1.5 Tesla magnetic resonance imaging scanners compared with 3.0 Tesla magnetic resonance imaging scanners: systematic review of clinical effectiveness. CADTH Technol Overv 2012; 2:e2201.
16. Eguchi A, Nakashima O, Okudaira S, Sugihara S, Kojiro M. Adenomatous hyperplasia in the vicinity of small hepatocellular carcinoma. Hepatology 1992; 15:843–848. [CrossRef]
17. Rohrer M, Bauer H, Mintorovitch J, Requardt M, Weinmann HJ. Comparison of magnetic properties of MRI contrast media solutions at different magnetic field strengths. Invest Radiol 2005; 40:715–724. [CrossRef]
18. Goshima S, Kanematsu M, Watanabe H, et al. Hepatic hemangioma and metastasis: differentiation with gadoxetate disodium-enhanced 3-T MRI. AJR Am J Roentgenol 2010; 195:941–946. [CrossRef]
19. Schuhmann-Giampieri G, Schmitt-Willich H, Press WR, Negishi C, Weinmann HJ, Speck U. Preclinical evaluation of Gd-EOB-DTPA as a contrast agent in MR imaging of the hepatobiliary system. Radiology 1992; 183:59–64. [CrossRef]
20. Itai Y, Ohtomo K, Kokubo T, et al. CT of hepatic masses: significance of prolonged and delayed enhancement. AJR Am J Roentgenol 1986; 146:729–733. [CrossRef]
21. Kang Y, Lee JM, Kim SH, Han JK, Choi BI. Intrahepatic mass-forming cholangiocarcinoma: enhancement patterns on gadoxetic acid-enhanced MR images. Radiology 2012; 264:751–760. [CrossRef]
22. Kitao A, Matsui O, Yoneda N, et al. The uptake transporter OATP8 expression decreases during multistep hepatocarcinogenesis: correlation with gadoxetic acid enhanced MR imaging. Eur Radiol 2011; 21:2056–2066. [CrossRef]
23. Doo KW, Lee CH, Choi JW, Lee J, Kim KA, Park CM. "Pseudo washout" sign in high-flow hepatic hemangioma on gadoxetic acid contrast-enhanced MRI mimicking hypervascular tumor. AJR Am J Roentgenol 2009; 193:W490–496. [CrossRef]
24. Grazioli L, Olivetti L, Fugazzola C, et al. The pseudocapsule in hepatocellular carcinoma: correlation between dynamic MR imaging and pathology. Eur Radiol 1999; 9:62–67. [CrossRef]
25. Nishie A, Tajima T, Asayama Y, et al. Diagnostic performance of apparent diffusion coefficient for predicting histological grade of hepatocellular carcinoma. Eur J Radiol 2011; 80:e29–33. [CrossRef]